REGISTRATION ANALYSIS AND INNER CALIBRATION OF A THREE CCD MULTISPECTRAL FRAME CAMERA

M. Galo, A. M. G. Tommaselli, J. K. Hasegawa, N. N. Imai

Dept. of Cartography, UNESP - Universidade Estadual Paulista, FCT, Rua Roberto Simonsen 305, CEP 19060-900, Presidente Prudente, SP – (galo, hasegawa, tomaseli, nnimai)@prudente.unesp.br

EuroCOW 2006 - ISPRS/EuroSDR Workshop

KEY WORDS: Band registration, Multispectral camera, Digital camera calibration, Interior Orientation Parameters, Subpixel point extraction, 3D reconstruction

ABSTRACT:

Several digital cameras are commercially available nowadays, with a broad range of characteristics. A category of cameras of special interest for airborne remote sensing aiming at agriculture and environmental applications is the multispectral camera. Among the available cameras with this feature there is the Multispectral DuncanTech MS3100 – CIR camera. This camera is composed by three CCD sensors, that capture the energy in the infra-red (IR), red (R) and green (G) spectral regions. Since between the camera lenses and each CCD array there are optical elements like prisms, filters, etc, some additional deviation in the bundle of rays are expected. Considering the features of the described camera, the aim of this paper is to perform the analysis of the band registration; the inner calibration for this camera, using a bundle adjustment with convergent images to estimate the Inner Orientation Parameters – IOP; and the quality of 3D reconstruction using different bands. To evaluate the registration between the channels, the coordinates of interest points are obtained by using a semi-automatic subpixel point extraction technique based on Förstner Operator and the discrepancies between the bands are computed and statistically evaluated. The preliminary results indicate that the smallest RMSE in the reconstruction of the 3D coordinates was obtained when the IR images were considered, followed by the original CIR - Color-InfraRed composition. Concerning the registration analysis, band miss-registration of about 0.5 pixels (in average) were obtained in the experiments. These discrepancies are significant, especially for those applications where multiband images and subpixel measurement are required.

1. INTRODUCTION

The use of digital cameras is growing in several applications. As example one can mention: agriculture, mapping, environment applications, security, and industrial inspection. A category of camera of special interest in some applications is the multispectral cameras. The interest in these cameras can be justified by the great amount of information about the objects of interest that can be extracted by analyzing the images, due to the broad camera spectral range.

The DuncanTech MS3100 – CIR (Color-InfraRed) can be mentioned as an example of multispectral frame camera. This camera is composed by three CCD sensors and between each CCD and the lenses there are optical elements like prisms, filters, etc, that cause the deviation of the incident energy to each sensor surface. In this camera each CCD sensor captures the energy in a specific region of the electromagnetic spectrum: Infra-Red (IR), Red (R) and Green (G).

Since the images in the Color-Infrared (CIR) mode are obtained by the composition of the information captured by the IR, R and G sensors, one aspect that must be assessed is the band registration.

Another important aspect to be considered is the camera calibration. Although the camera calibration is a subject extensively explored by the photogrammetric and computer vision communities, the development of the technology and the availability of systems and imaging sensors with different characteristics made this topic actual and of special interest. The terms of reference of the EuroSDR - European Spatial Data Research (EuroSDR, 2004; Cramer, 2004) commissions and the questions addressed by the ASPRS Camera Calibration Panel (ASPRS, 2000) validates this concern.

By analyzing the mission and terms of reference of the EuroSDR commissions, several aspects can be observed and topics as sensor calibration, sensors intercalibration and sensor's quality are included. In the ASPRS Camera Calibration Panel, the purpose of geometric calibration; methodologies; technologic aspects related to sensor, camera types and sensor integrations; current practices; infrastructure; and standardizations are discussed. Considering these points of interest and the diversity of aspects that should be studied, ranging from sensor geometry to standardization of operations and temporal stability of the inner parameters, one of these aspects is the evaluation of internal geometry of cameras with more than one CCD sensor. As example of this type of camera one can mention the digital frame camera DuncanTech MS3100 – CIR.

Since this camera is composed by three CCD sensors, the aim of this paper is to evaluate the following aspects: bands registration, the inner orientation parameters for different bands and also for CIR composition and the quality of 3D reconstruction using images from different bands. It is relevant to mention that this kind of evaluation is important only for those applications in which the images will be used for metric applications and where subpixel measurements will be considered.

2. FEATURES OF THE MULTISPECTRAL CAMERA USED IN THE EXPERIMENTS

In this section some characteristics of the multispectral digital frame camera DuncanTech MS3100 – CIR (see Figure 1) will be show.

Figure 1. Multispectral DuncanTech MS3100 camera. (Adapted from Redlake, 2003)

This camera has three array sensors based on CCD – Charge Couple Device technology. Each array has the dimension 6.4 mm (h) ×4.8 mm (v). Between the lenses and each CCD sensor there are optical elements as prisms, filters and dichroic coats (Hi-Tech, 2005), as can be seen in Figure 2. The two dichroic coats split the energy in specific wavelengths (infra-red (IR), red (R) and green (G)).

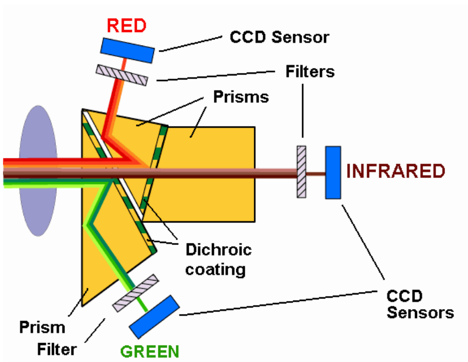

Figure 2. The internal geometry and main components of the optical system of the DuncanTech MS3100 – CIR camera. (Adapted from Hi-Tech, 2005)

Some details related to camera and the lenses used in the experiments are:

- Camera: Multiespectral DuncanTech;
- Model: MS3100 – CIR (Part Nº. 35135-60, Serial Nº. 152);
- Sensor: 3 CCDs (1/2” – 6.4×4.8 mm);
- Image size: 1392 (h)x1039 (v);
- Objective: Tokina AT-X Pro (Serial Nº 6301854), ϕ77 mm;
- Aspherical lenses;
- Nominal focal length: 17 mm.

3. REGISTRATION ANALYSIS

The analysis described in this section is performed in order to evaluate the registration between the bands IR, R and G. The most straightforward model to consider is the shift between the bands and to ensure that the shift between bands are estimated accurately, it is necessary to use a measurement technique that gives accurate image coordinates of points.

3.1 Images and measurements

The images used in the experiments were acquired over a flat test field, as shown in Figure 3.

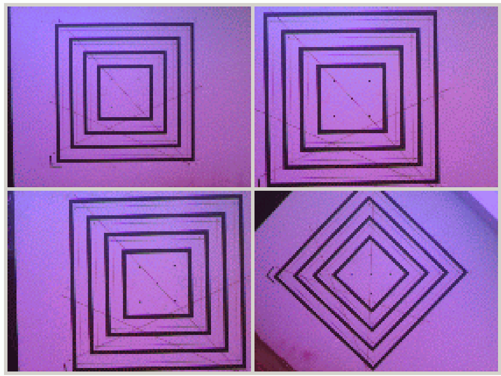

Figure 3. Images in CIR mode used in the registration analysis.

As can be observed, there are some black wide strips in the test field, whose locations were measured using a metallic scale. In this way there are well defined corners, which can be measured in the images with subpixel accuracy. The principle used to obtain the corner position is based on the fact that the corner is located at the intersection of vectors that are orthogonal to the directions of maximum gradient at the edges, as show in Figure 4.

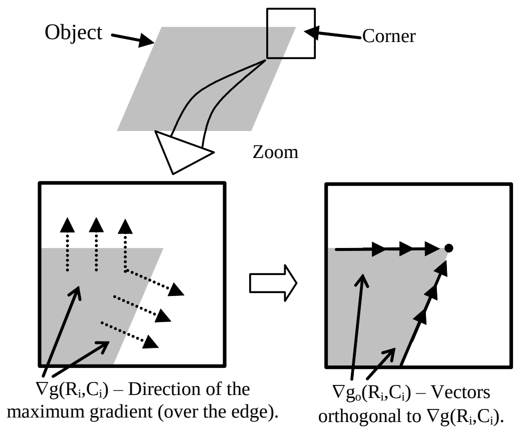

Figure 4. Subpixel corner estimation principle based on the intersections of vector orthogonal to the maximum gradient vectors $\nabla g(R_i,C_i)$. (Adapted from Galo and Tozzi, 2002)

Assuming that the direction of maximum gradient at one pixel (Row,Column)=(R,C) is $\nabla g(R,C)$ and that the vector orthogonal to this vector is $\nabla g_o(R,C)$, the intersection of all vector $\nabla g_o(R,C)$ in a neighborhood of one corner point allows the estimation of this corner position. Representing one generic point i on the edge by (R_i,C_j), the corner position to be determined by (R_o,C_o), and considering the straight line equation in polar mode, the following equation can be written:

$$n_i = \rho(R_i, C_i) - R_o \cos\theta - C_o \mathrm{sen}\theta = 0\,, \qquad (1)$$

where n_i represents the distance between the point (L_o,C_o) and the straight line defined by (ρ, θ), as shown in Figure 5.

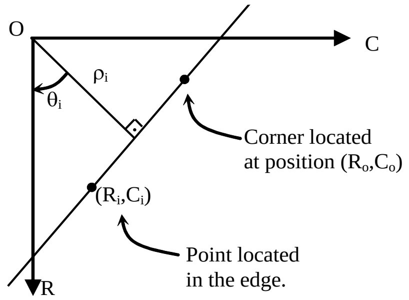

Figure 5. Corner position at (R_o,C_o) and edge passing through the point (R_i,C_i).

If inside one window with m elements one corner exists, whose position is (L_o,C_o), one system of equations can be written by using Equation 1, where the parameters R_o and C_o can be estimated using a LSM – Least Square Method. Considering that only edge points should be used to obtain the corner position, the magnitude of the gradient can be used as a weight factor, as proposed by Haralick and Shapiro (1993, p. 336). Under these assumptions, the following function can be written:

$$\Omega(\hat{R}_o,\hat{C}_o)=\sum_{i=1}^{m}\left(\rho(R_i,C_i)-\hat{R}_o\cos\theta_i-\hat{C}_o \mathrm{sen}\theta_i\right)^2 w_i \cdot \quad (2)$$

where g_{Ri} and g_{Ci} are the components of the gradient along rows and columns, respectively, and $w_i=\|\nabla g_i\|^2=g_{Ri}^2+g_{Ci}^2$. The corner position $(\hat{R}_o,\hat{C}_o)$ can be estimated considering that this point coordinates minimizes the function 2. This development can be seen in Haralick and Shapiro (1993, p. 341) and the solution of this system leads to:

$$\begin{bmatrix}\hat{R}_o\\ \hat{C}_o\end{bmatrix}=\begin{bmatrix}\sum g_{Ri}^2 & \sum g_{Ri}g_{Ci}\\ \sum g_{Ci}g_{Ri} & \sum g_{Ci}^2\end{bmatrix}^{-1}\begin{bmatrix}\sum\left(\mathrm{Ri}\,g_{Ri}^2+\mathrm{Ci}\,g_{Ri}g_{Ci}\right)\\ \sum\left(\mathrm{Ci}\,g_{Ci}^2+\mathrm{Ri}\,g_{Ri}g_{Ci}\right)\end{bmatrix}.(3)$$

The result of Equation 3 depends on the inversion of one 2x2 matrix. This matrix can be associated with the Covariance matrix of the estimation process, which can be used to obtain the error ellipses associated to the corner position. By computing the dimension and eccentricity of the error ellipse associate to each point it is possible to classify this point (Haralick and Shapiro, 1993, p. 341). It is relevant to mention that this matrix is exactly the matrix used by the Förstner operator, as can be observed in Förstner (1986, p. 136), Luhmann and Altrogge (1986, p. 467) and Rohr (1997, p. 220), for example. The described method is based on Haralick and Shapiro (1993) and Förstner (1986), and, after some changes, can be used to locate the centre of circular symmetry as well.

Figure 6 depicts an example of application of the described approach to detect two corners. It is possible to see two distinct corners in the R and IR bands.

In these images the positions measured manually are represented by a (+) symbol. The symbol (*) is used to show the position in the R band, the triangle is used to show the position obtained in IR band and the circle in the G band.

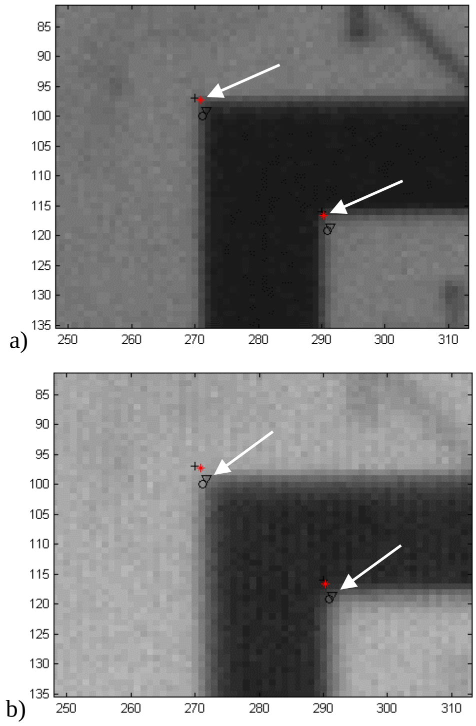

Figure 6. Corner points semi-automatically extract in R band (a) and in IR band (b).

3.2 Statistical Analysis of the Registration

The method described in the previous section was implemented and used to obtain points with subpixel accuracy. First, the images were acquired in a CIR mode and these images were splited in different files, corresponding to IR, R and G bands. Using the manual screen pointing method, all corners were measured in the CIR images. The positions obtained manually were used as approximated position of the corners, aiming the estimation of corners with subpixel accuracy in all the images by using the approach described in section 3.1.

This procedure was performed in the four images shown in Figure 3 and discrepancies between the bands were computed. The results are summarized in Table 1.

Discrepancies between the bands IR and R		
	ΔC [pixel]	**ΔR [pixel]**
Average and standard deviation	**-0.783** ± 0.304	**-1.466** ± 0.277
Minimum and maximum	-1.734 -0.075	-2.136 -0.651
Discrepancies between the bands IR and G		
Average and standard deviation	**-0.678** ± 0.270	**0.600** ± 0.232
Minimum and maximum	-1.425 0.058	0.031 1.609
Number of points	N=138	

Table 1. Basic statistics related to the discrepancies in rows and columns for the bands IR-R and IR-G.

The statistics shown in Table 1 were used to compute the confidence intervals for both translations (ΔC and ΔR) considering a probability of 99%. The results of these computations allow to conclude that significant translations exist since the null value do not belong to these confidence intervals.

Based on these results the estimated translations were used to register the bands R and G to the band IR. This registration of bands was performed using the parameters obtained in the Table 1 with bilinear resampling. Figure 6 shows the images before and after registration.

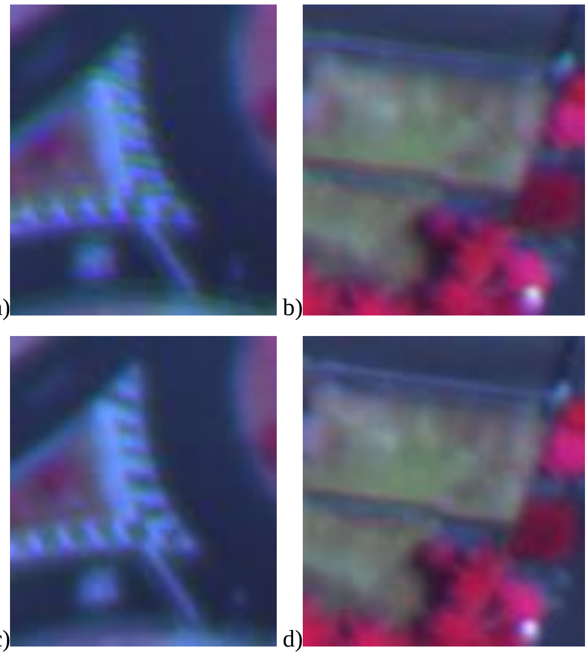

Figure 6. Two details of one aerial image before (a and b) and after (c and d) the bands registration.

By observing Figure 6 it is possible to see that the quality of the image in CIR mode is improved after the bands registration.

4. INNER ORIENTATION PARAMETERS ANALYSYS

In this section the inner orientation parameters of the camera are analyzed and the following aspects are considered: the influence of IOP and the effect of subpixel measurements; the behavior of the IOP for different bands, and the quality of 3D reconstructions using only 3 images.

The experiments described in this section were performed using in-house developed software (CC – Camera Calibration) which is based on colinearity equations as fundamental model. This software allows choosing the additional parameters to be included in the adjustment computations (Galo, 2003). The parameters that can be chosen are the camera focal length (c); principal point position (x_0, y_0); radial lens distortion coefficients (k_1, k_2, k_3); decentring distortion coefficients (P_1, P_2) and affinity parameters (A, B) (Moniwa, 1972).

Ten images were measured in order to achieve these experiments, using the same test field described in section 3. To minimize the effect of correlation between some inner and exterior orientation parameters some convergent images were used.

4.1 Influence of IOP and subpixel measurement

In the first experiment well defined points (corners) were manually measured on ten CIR images. Using these coordinates different groups of IOP were estimated. Table 2 presents the combinations considered. Due to the lack of space only the standard deviation of the camera constant is shown for each option.

Option	**IOP Inner Orientation Parameters**	σ_c(pixels)
#1	c x_0 y_0 k_1 k_2 k_3 P_1 P_2 A B	8.964
#2	c x_0 y_0 k_1 k_2 k_3 P_1 P_2	8.916
#3	c x_0 y_0 k_1 k_2 k_3	8.955
#4	c x_0 y_0 k_1	**8.736**
#5	c x_0 y_0	10.077
#6	c x_0 y_0 k_1 P_1 P_2	**8.739**
#7	c x_0 y_0 k_1 A B	8.778

Table 2. IOP considered and the estimated standard deviation of the camera constant (σ_c).

As can be seen in Table 2, the smallests σ_c correspond to the options #4 and #6. Using the same images but with corners measured by using the semi-automatic approach described in sections 3.1 these calibrations were reprocessed. Some results related to the option #6 are shown in Figure 7.

a) IOP and residuals (in pixels) using option #6 with manual point extraction

c = 16.5512 mm +- 0.4107E-01 (σ_c= 8.739 pixel)
x_0 = 0.0419 mm +- 0.3678E-01 (Column 704.418)
y_0 = -0.2115 mm +- 0.6677E-01 (Row 564.009)
k_1 = -.3830136E-03 mm^{-2} +- 0.2745E-04
P_1 = 0.8275310E-04 mm^{-1} +- 0.5121E-04
P_2 = -.3607730E-04 mm^{-1} +- 0.6168E-04

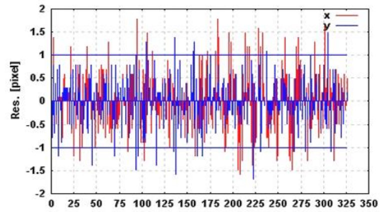

b) IOP and residuals (in pixels) using option #6 with semi-automatic point extraction

c = 16.5739 mm +- 0.2739E-01 (σ_c= 5.828 pixel)
x_0 = -0.0992 mm +- 0.2453E-01 (Column 674.387)
y_0 = -0.0137 mm +- 0.4417E-01 (Row 521.905)
k_1 = -.3761238E-03 mm^{-2} +- 0.1823E-04
P_1 = -.7432887E-04 mm^{-1} +- 0.3470E-04
P_2 = 0.4913056E-04 mm^{-1} +- 0.4128E-04

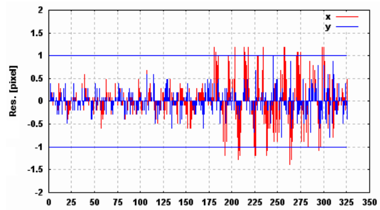

Figure 7. Parameters and residuals in coordinates (x,y) for the group of parameters c x_0 y_0 k_1 P_1 P_2 when manual (a) and semi-automatic measurements are considered (b).

Analyzing the results it is possible to observe the reduction in the standard deviation in the IOP. It is also possible to observe that part of the residuals suffers great reduction when a subpixel measurement technique was considered. Although the images are not shown, these reductions were mostly observed in non-convergent images. From these results it is possible to presume that the quality improvement due to the use of subpixel algorithm is more significant in non-convergent images.

The results presented related to subpixel measurements were obtained using 15x15 pixels windows around the approximated corner position (manually measured).

4.2 Evaluation of IOP for different bands

In this section the estimated IOP for the same group of images, in CIR mode and for each band separately are presented. For the single bands all the computations were made using subpixel point extraction and for the case of CIR mode the manual and subpixel measurement were also used. The results shown correspond only to the subpixel measurements.

In Table 3 and 4 the IOP for each band and for the CIR images are shown. In these tables the groups of parameters are: (c, x_0, y_0, k_1) and (c, x_0, y_0, k_1, P_1, P_2).

IOP	CIR mode	IR band	R band	G band
c (mm)	16.5737 ± 0.0275 5.84 pixel	16.5442 ± **0.0274** 5.84 pixel	16.5495 ± 0.0278 5.92 pixel	16.4966 ± 0.0325 6.93 pixel
x_0 (mm)	-0.0532 ± 0.0208	-0.1275 ± **0.0207**	-0.0497 ± 0.0211	-0.1735 ± 0.0248
y_0 (mm)	-0.0561 ± 0.0282	-0.0485 ± **0.0280**	-0.0133 ± 0.0282	-0.0228 ± 0.0332
k_1 (mm^{-2})	-3.727e-4 ± **1.82e-5**	-3.719e-4 ± 1.83e-5	-3.639e-4 ± 1.85e-5	-3.683e-4 ± 2.19e-5

Table 3. IOP for different bands and the group (c, x_0, y_0, k_1).

IOP	CIR mode	IR band	R band	G band
c (mm)	16.5739 ± **0.0274** 5.83 pixel	16.5444 ± **0.0274** 5.83 pixel	16.5484 ± 0.0278 5.92 pixel	16.4997 ± 0.0325 6.92 pixel
x_0 (mm)	-0.0992 ± **0.0245**	-0.1627 ± **0.0245**	-0.0704 ± 0.0254	-0.1836 ± 0.0293
y_0 (mm)	-0.0137 ± 0.0442	-0.0001 ± **0.0441**	-0.0436 ± 0.0452	0.0673 ± 0.0520
k_1 (mm^{-2})	-3.761e-4 ± **1.82e-5**	-3.741e-4 ± 1.83e-5	-3.640e-4 ± 1.86e-5	-3.716e-4 ± 2.19e-5
P_1 (mm^{-1})	-7.43e-5 ± **3.47**e-5	-5.43e-5 ± 3.48e-5	-3.90e-5 ± 3.56e-5	-0.86e-5 ± 4.18e-5
P_2 (mm^{-1})	4.91e-5 **± 4.13e-5**	5.68e-5 ± 4.14e-5	-4.07e-5 ± 4.26e-5	11.28e-5 ± 4.95e-5

Table 4. IOP for different bands and the group (c, x_0, y_0, k_1, P_1, P_2).

In this experiment, and also in the experiment show in section 4.1, the parameters c and k_1 are more stable between the experiments when compared to x_0, y_0, P_1 and P_2. In Figure 8 it is possible to observe the principal point position for the experiments presented in Table 4. The principal point position obtained from manually measured images is included in Figure 8, although it was not shown in table 4.

In Tables 3 and 4 the smallests values of standard deviation (σ) were highlighted, for each estimated IOP. It is possible to observe that the smallest values of σ correspond to the use of IR band and the CIR composition. It is thus coherent to consider that for metric purposes, when one band or the composition is chosen, the IOP should be compatible to this choice. To visualize the magnitude of the radial and decentring distortions Figure 9 is shown.

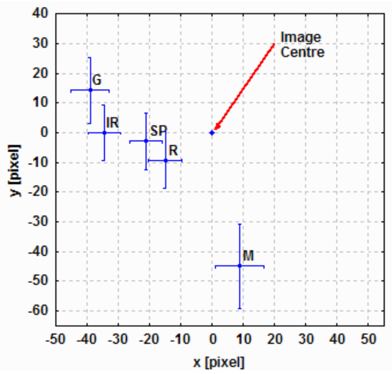

Figure 8. Principal point position for different bands (IR, R and G) and also for the image in CIR mode, considering subpixel (SP) and manual (M) extraction.

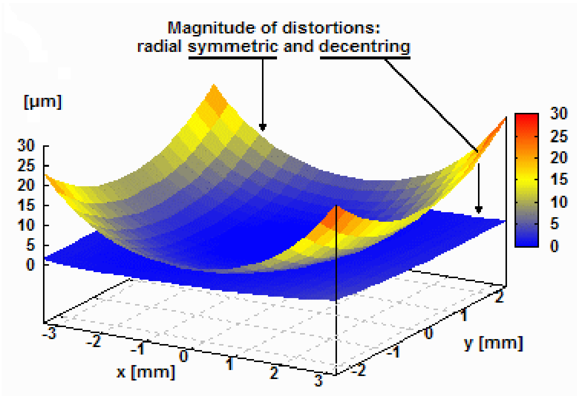

Figure 9. Magnitude of radial and decentring distortions for IR band.

By observing the surface in Figure 9 it is possible to verify the great influence of radial symmetric distortions when comparing to decentring distortions.

In the previous sections only the aspects related to the registration between the bands and the IOP for different bands were studied. In the next section some results regarding the 3D reconstruction are presented and discussed.

4.3 The accuracy of 3D reconstruction

Using only three images, as shown in Figure 10, the 3D reconstruction of 28 points was performed. From these 28 points, 5 were used as control points and 23 as check points. In these solutions, the IOP were constrained according to the IOP group and according to the set of image used. In Figure 11 the relative position of the test field and three images (CP1, CP2 and CP3) are shown.

The RMS errors were computed for XY and Z components and to obtain a relative error, the ratio between the RMS and the average distance ($\overline{D}$) was computed and shown in Tables 5 and 6.

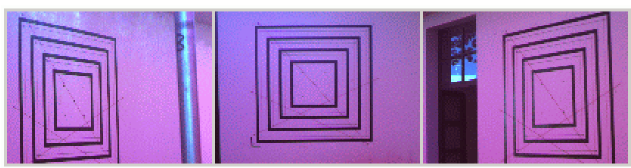

Figure 10. Images used to verify the 3D reconstruction.

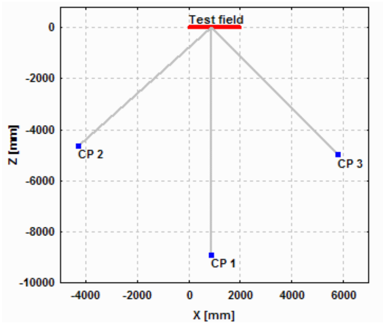

Figure 11. Camera positions related to the test field.

	$RMS_Z/\overline{D}$ c x_0 y_0 k_1	$RMS_Z/\overline{D}$ c x_0 y_0 k_1 A B	$RMS_Z/\overline{D}$ c x_0 y_0 k_1 P_1 P_2
CIR (P)	1/2262	1/2263	1/1956
CIR (SP)	1/2657	1/2676	1/2710
IR	**1/2879**	**1/2902**	**1/2912**
R	1/2422	1/2423	1/2447
G	1/2593	1/2625	1/2592

Table 5. Relative error (RMS/$\overline{D}$) in Z component.

	$EMQ_{XY}/\overline{D}$ c x_0 y_0 k_1	$EMQ_{XY}/\overline{D}$ c x_0 y_0 k_1 A B	$EMQ_{XY}/\overline{D}$ c x_0 y_0 k_1 P_1 P_2
CIR (P)	1/2952	1/2964	1/1861
CIR (SP)	1/4753	1/5015	1/4892
IR	**1/5428**	**1/5722**	**1/5640**
R	1/4958	1/4913	1/4975
G	1/3580	1/4058	1/3684

Table 6. Relative error (RMS/$\overline{D}$) in XY plane.

As can be observed in these tables, it is possible to see that smallest relative error are obtained when the IR band is considered, for the groups of parameters tested.

5. FINAL REMARKS AND CONCLUSIONS

In this work the analysis of registration between the bands, the IOP and also the 3D reconstruction using images obtained by a 3CCD camera were presented. For the experiments, a semi-automatic point extraction approach based on Förtner Operator was used, aiming the point positioning with subpixel accuracy

The analysis of discrepancies between the bands IR-R and IR-G allows to conclude that the discrepancies obtained are significant. So, in applications were high metric quality is required, it is relevant to verify the registration between the bands when cameras with more than one CCD is used. The authors recommend to consider different model in the registrations analysis (e.g., rigid body or Helmet transformation) as a suggestion for future work.

Another aspect studied was the IOP for each band. Considering the standard deviation of the parameters, the best results were obtained using the following groups of parameters: (c, x_0, y_0 and k_1); (c, x_0, y_0, k_1, P_1 and P_2) and (c, x_0, y_0, k_1, A and B).

The use of subpixel point extraction techniques improves the calibration results and also 3D reconstruction. This can be observed by considering both the standard deviation and the RMS error over the check points.

The results showed that c and k_1 are the more stables IOP. The others parameters changes more significantly when different bands are considered. The analysis of the relative error indicates that better results in 3D reconstruction are obtained when the images in IR mode are considered.

Although some aspects and concepts are suitable for others sensors, it is relevant to mention that part of the conclusions are valid only for the camera used in the experiments.

REFERENCES

ASPRS – The Imaging and Geospatial Information Society, Sensing, 2000. *Camera Calibration Panel Report*, sponsored by USGS, January, 2000. http://www.asprs.org/asprs/news/archive/final_report.html (accessed 07 Apr. 2005)

Cramer, M., 2004. EUROSDR Network on digital camera calibration. In.: *XX*[th] *ISPRS Congress*, Istanbul, 2004, Commission VI, July.

EuroSDR - European Spatial Data Research, 2004. *Rolling Research Plan 2004 - 2006*. http://www.eurosdr.org (accessed 01 Oct. 2004)

Förstner, W., 1986. A feature based correspondence algorithm for image matching. In: *IAPRS - International Archives of Photogrammetry and Remote Sensing*, Vol. XXVI (3/3), pp. 150-166.

Galo, M., 1993. *Calibração e aplicação de câmaras digitais*. Dissertação de Mestrado, Curso de Pós-Graduação em Ciências Geodésicas, Universidade Federal do Paraná, Curitiba - PR, 151p.

Galo, M.; Tozzi, C. L., 2002. Extração de pontos com acurácia subpixel em imagens digitais. In: Mitishita, Edson Aparecido. (Org.). *Série em Ciências Geodésicas - Pesquisa em Ciências Geodésicas*. Curitiba, v. 2, p. 289-313. ISBN: 85-88783-03-7.

Haralick, R. M.; Shapiro, L. G., 1993. *Computer and robot vision - Vol. II*. Addison-Wesley Publishing Company, Reading,. 630 p.

Hi-Tech Electronics, 2005. *Spectral Configuration Guide for DuncanTech 3-CCD Cameras*. http://www.hitech.com.sg. (accessed 01 Feb. 2005)

Luhmann, T.; Altrogge, G., 1986. Interest-operator for image matching. In: *IAPRS - International Archives of Photogrammetry and Remote Sensing*. Vol. XXVI (3/2), pp. 459-474.

Moniwa, H., 1972. *Analytical camera calibration for close-range photogrammetry*. New Brunswick, Thesis, Master of Science, University of New Brunswick, 104p.

Redlake MASD, 2003. MegaPlus® MS3100 Multi-Spectral Câmera. http://www.redlake.com (accessed 06 Dec. 2004)

Rohr, K., 1997. On 3D differential operators for detecting point landmarks. *Image and Vision Computing*, Vol. 15, pp. 219-233.

ACKNOWLEDGEMENTS

The authors express their acknowledgements to the following organizations:

- CNPq - Conselho Nacional de Desenvolvimento Científico e Tecnológico (Projects 481047/2004-2 and 475932/2003-0);
- FAPESP - Fundação de Amparo à Pesquisa do Estado de São Paulo (Project 1997/10956-0).